STRUCTURAL CONTROL AND HEALTH MONITORING
Struct. Control Health Monit. (2011)
Published online in Wiley Online Library (wileyonlinelibrary.com). DOI: 10.1002/stc.471

Implementation of passive and active vibration control on an in-service footbridge

Carlos M. Casado[1], Iván M. Díaz[2,*,†], Jesús de Sebastián[1], Alfonso V. Poncela[3] and Antolín Lorenzana[3]

[1]*CARTIF Centro Tecnológico, Parque Tecnológico de Boecillo, Parcela 205, E-47151, Boecillo, Valladolid, Spain*
[2]*Escuela Técnica Superior de Ingenieros Industriales, Universidad de Castilla-La Mancha, Edificio Politécnico, Av. Camilo José Cela s/n, E-13071, Ciudad Real, Spain*
[3]*ITAP, Escuela de Ingenierías Industriales, Universidad de Valladolid, Paseo del Cauce 59, E-47011, Valladolid, Spain*

SUMMARY

The current trend toward lighter and slender pedestrian structures, with new aesthetic requirements and high-performance materials, has resulted in structures with increased susceptibility to vibration. Notable vibrations under human-induced excitations might appear, and the vibration serviceability requirements might not be accomplished. The Valladolid Science Museum Footbridge (Spain) is an example of a lively structure that might achieve excessive vertical acceleration under walking or running excitation. The control of excessive footbridge vibrations via passive and active devices is dealt with in this work. More specifically, this paper is concerned with the design and experimental implementation of a passive tuned mass damper (TMD) and an active mass damper (AMD) to mitigate human-induced vibrations on this in-service footbridge. The TMD, with a mass ratio of 1%, is designed by a numerical method based on H_∞ controllers. The AMD consists of a proof-mass actuator, with a mass ratio of approximately 0.2%, controlled by a strategy based on acceleration feedback with a phase-lag network. The performance of both devices has been assessed. Copyright © 2011 John Wiley & Sons, Ltd.

Received 20 October 2010; Revised 14 March 2011; Accepted 3 May 2011

KEY WORDS: footbridges; vibration control; human-induced vibrations; active control; passive control

1. INTRODUCTION

Advances in structural technologies, including construction materials and design technologies, are leading to the design of lighter and slender structures with fewer non-structural elements that are usually cost-effective and appealing from an architectural point of view. However, these structures present much less inherent damping and lower natural frequencies than in the past and hence are more susceptible to excitation by human users. Examples of notable vibrations under human-induced excitations have been reported in footbridges, office buildings, shopping malls and sport stadia, amongst others structures [1–3]. Such vibrations can cause a serviceability problem in terms of disturbing the users, but they do rarely affect the fatigue life or safety of structures.

Concerning footbridges, in particular, urban footbridges, which are usually tourist landmarks, architects and engineers often employ highly performing materials and sophisticated design techniques leading to lightweight and slender footbridges that might be quite lively [4,5]. Solutions to overcome this vibration serviceability problem might be the following: (i) designing in order to avoid natural frequencies into the habitual pacing rate of walking or running; (ii) stiffening the structure in the appropriate direction resulting in significant design modifications; (iii) increasing the weight of the

*Correspondence to: Iván M. Díaz, Escuela Técnica Superior de Ingenieros Industriales, Universidad de Castilla-La Mancha, Edificio Politécnico, Av. Camilo José Cela s/n, E-13071, Ciudad Real, Spain.
†E-mail: Ivan.Munoz@uclm.es

structure to reduce the human influence, a proportional increase of stiffness being also necessary; and (iv) increasing the damping of the structure with special devices. Taking into account that stiffening the structure and increasing the mass are usually complicated and involve significant structural and non-structural changes, the alternative option of including damping devices to the structure seems to be the easiest way of improving the vibration performance of footbridges. Typical passive damping systems [6] are metallic dampers, friction dampers, visco-elastic dampers, viscous dampers, tuned mass dampers (TMDs) and tuned liquid dampers (TLDs). Among passive control devices available for implementation in footbridges, TMDs [7,8] (including parallel multiple TMDs [9] and series multiple TMDs [10]), TLDs [11] and fluid–viscous dampers are the most effective and, hence, the usual adopted solution [12].

An alternative procedure to cancel footbridge vibrations is the use of active devices. Moutinho *et al.* [13] have recently implemented an active vibration control (AVC) on a stress-ribbon footbridge using a proof-mass actuator together with direct velocity feedback control (DVFC) with saturation. This actuator generates inertial forces in the structure without need for a fixed reference. The velocity output, which is obtained by an integrator circuit applied to the measured acceleration response, is multiplied by a gain and feeds back to a collocated actuator. The term collocated means that the actuator and sensor are located physically at the same point on the structure. The merits of this method are its robustness to spillover effects due to high-order unmodelled dynamics and that it is unconditionally stable in the absence of actuator and sensor (accelerometer with an integrator circuit) dynamics [14]. Nonetheless, when such dynamics are considered, the stability for high gains is no longer guaranteed, and the system can exhibit limit cycle behaviour, which is not desirable since it could result in dramatic effects on the system performance and its components [15]. Then, DVFC with saturation is not such a desirable solution. Generally, the actuator and sensor dynamics influence the system dynamics and have to be considered in the design process of the AVC system. If the interaction between sensor/actuator and structure dynamics is not taken into account, the AVC system might exhibit poor stability margins, be sensitive to parameter uncertainties and be ineffective. Díaz and Reynolds [16] have recently proposed a control strategy based on a phase-lag compensator applied to the structure acceleration, which is usually the actual magnitude measured. This compensator accounts for the interaction between the structure and the actuator and sensor dynamics in such a way that the closed-loop system shows desirable properties. Such properties are high damping for the fundamental vibration mode of the structure and high stability margins. Both properties lead to a closed-loop system robust with respect to stability and performance [17]. This control law is completed by the following: (i) a high-pass filter, applied to the output of the phase-lag compensator, designed to avoid actuator stroke saturation due to low-frequency components and (ii) a saturation nonlinearity applied to the control signal to avoid actuator force overloading at any frequency. This methodology will be referred as to compensated acceleration feedback control (CAFC) from this point onwards.

This paper presents the practical implementation of inertial mass-based damping devices, passive and active, in order to cancel excessive vertical vibrations on a footbridge. More specifically, this paper addresses the design and implementation of a passive TMD and an active mass damper (AMD) on the Valladolid Science Museum Footbridge (Spain). This is a structure composed of four spans. One of them, which is a 51-m long steel structure, is considered by its users to be quite lively. The first bending mode of this span is at approximately 3.5 Hz in such a way that it might be excited by the second harmonic of walking and by the first harmonic of running. It was decided to install the designed damping devices at the point in which the first bending mode shape has its maximum value, which is close to the mid-span. The TMD, with an inertial mass ratio of approximately 1% of the modal mass of the targeted vibration mode, was designed by a numerical method based on H_∞ controllers [18]. The mass value of 1% of modal mass was found to be enough to keep the vibration level for a synchronised walker and runner within most of the limit values provided by current codes [12]. The H_∞-based method used for the TMD design obtains the damping ratio and natural frequency of the TMD through the minimisation of the H_∞-norm of the transfer function between the structure acceleration (output) and the force disturbance (input). H_∞-based techniques are usually recommended for structures excited by loads exhibiting mainly periodical time components, such as those generated by human activities like walking or running. The AMD consisted of a commercial electrodynamic inertial actuator (with an inertial mass of around 0.15% of the modal mass) controlled via CAFC [16].

DOI: 10.1002/stc

Some preliminary results obtained from the AVC strategy were presented in [19]. The design of both devices has been carried out using methodologies developed by some of the authors of the present paper [16,18] and applied to the Valladolid Science Museum Footbridge, which is an example of a flexible in-service footbridge. The performance of both devices is evaluated in this paper.

This paper continues with the description of the test structure, the identification of its modal parameters and the vibration serviceability assessment in the context of current codes. In section 3, the design and mechanical development of the TMD are described. The design and development of the AMD are presented in section 4. The experimental results conducted in order to assess the performance of both devices is presented in section 5. Several loading scenarios, involving walking, running and jumping tests, were considered with and without damping devices. Finally, some discussions and conclusions, together with suggestions for future work, are given in section 6.

2. STRUCTURE DYNAMICS AND SERVICEABILITY ASSESSMENT

This section describes the test structure and the identification of its modal parameters. This identification consisted in the operational modal analysis (OMA) of the liveliest span and obtaining the frequency response function (FRF) at the point of maximum amplitude of the first bending mode. It was observed that the natural frequency of this mode falls into the considered critical frequencies in most codes and standards for footbridge dynamic design. Thus, limit values of acceleration responses were checked for a synchronised walker and runner.

2.1. Description of the structure

The test structure, sited in Valladolid (Spain), is a footbridge that creates a pedestrian link over The Pisuerga River between the Science Museum and the city centre (see Figure 1). This bridge, built in 2004, is a 234-m truss structure composed of four spans: three made of tubular steel beams and one made of white concrete, all of them with a timber walkway. The main span (span 3 in Figure 1), with post-tensioning by two external cable systems (transversal and longitudinal), is 111 m; the second span (span 2 from this point onwards) is 51 m, and the other two spans are shorter and stiffer [20]. The external cable systems of span 3 have both aesthetical reasons (the original design by the architect José Rafael Moneo was based on the form of a fish basket) and structural reasons (making span 3 stiffer [21]).

Because of its slenderness, this footbridge, especially span 2, represents a typical lightweight structure sensitive to dynamic excitations produced by pedestrians. Annoying levels of vibration are sometimes perceived in span 2 (Figure 2). Special attention was paid to the point of maximum amplitude of the first bending mode since the vibration perception is acute at this point, particularly when runners cross the bridge. Therefore, it was decided to study the dynamic properties of this span and implement vibration control devices.

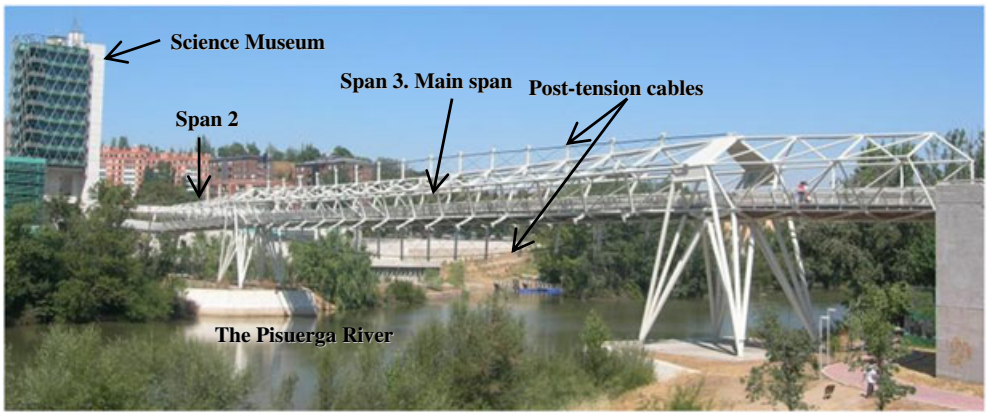

Figure 1. General view of the test structure.

DOI: 10.1002/stc

Figure 2. View of span 2.

2.2. Modal parameters identification

The OMA of span 2 was carried out in order to obtain the natural frequencies, damping ratios and modal shapes of the lower vibration modes. Additionally, since the first vibration mode (first bending mode at 3.5 Hz) was the most likely to be excited by human motions, it was decided to obtain also a high-quality FRF at the point of maximum amplitude and thus identify its modal properties, particularly its modal mass which is needed for the TMD tuning.

The OMA was carried out with five roving and two reference accelerometers (MMF-KS48C-1000 mV/g (Metra Mess - und Frequenzetechnik, Radebeul, Germany)). Preliminary spectral analyses and time history recordings indicated that the vertical vibration was considerably higher than the horizontal one; thus, only vertical response measurements were performed. A measurement grid of three longitudinal lines with nine equidistant test points was considered, resulting in 27 test points. Five setups with an acquisition time of 720 s and a sampling frequency of 100 Hz were recorded. Thus, it was expected to successfully identify vibration modes up to 30 Hz. The modal parameter estimation was carried out using the ARTEMIS suite of software (Structural Vibration Solutions A/S, Aalborg East, Denmark) [22]. In particular, frequency domain methods (frequency domain decomposition (FDD), enhanced frequency domain decomposition (EFDD) and curve-fit frequency domain decomposition (CFDD)) were used. Table I shows the modal parameters estimated through the OMA for the first four vibration modes. Figure 3 shows the corresponding estimated modal shapes.

Frequency response functions between the structure acceleration and the input force were obtained at the middle of the transversal steel beam sited closest to the point of maximum value of the first vibration mode. Firstly, a chirp signal with frequency content between 3 and 4 Hz was used to excite strongly the first vibration mode. The force was generated by an APS Dynamics Model 400 electrodynamic shaker (APS Dynamics, Inc., California Office San Juan Capistrano, CA, USA) operated in inertial mode and placed on the middle of the transversal beam (Figure 4a). The structure acceleration was measured by a piezoelectric accelerometer (as those used for the OMA) mounted by a magnet underneath the same transversal steel beam (Figure 4b). This point will be called control point from now on since the damping devices were installed here. The force induced by the shaker was estimated by measuring the acceleration of the inertial mass and multiplying this by the magnitude of

Table I. Natural frequencies and damping ratios identified by the OMA.

		Mode 1	Mode 2	Mode 3	Mode 4
FDD	Frequency (Hz)	3.516	6.250	7.373	9.351
	Damping ratio (%)	—	—	—	—
EFDD	Frequency (Hz)	3.506	6.278	7.386	9.365
	Damping ratio (%)	0.7221	0.4167	0.6571	0.5528
CFDD	Frequency (Hz)	3.508	6.274	7.389	9.367
	Damping ratio (%)	0.7984	0.2599	0.4319	0.3869

DOI: 10.1002/stc

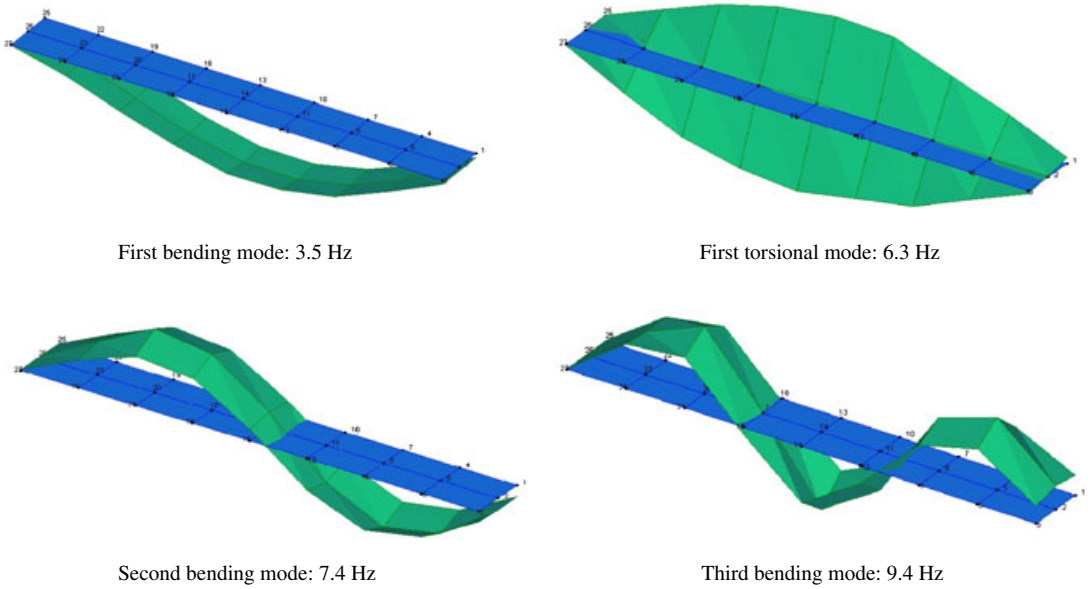

First bending mode: 3.5 Hz

First torsional mode: 6.3 Hz

Second bending mode: 7.4 Hz

Third bending mode: 9.4 Hz

Figure 3. Estimated modal shapes.

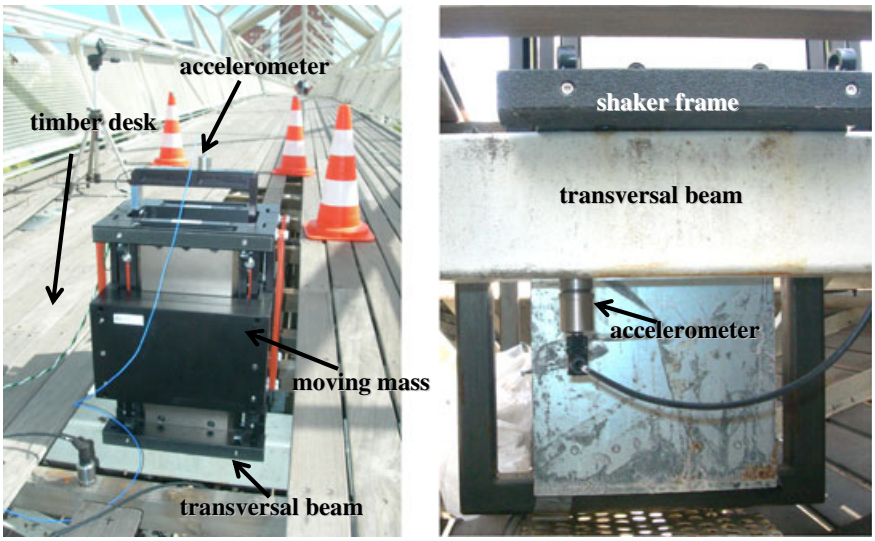

(a) (b)

Figure 4. (a) APS Electro-Seis Dynamic Shaker 400 placed on a transversal steel beam. (b) Accelerometer magnetically mounted under the timber walkway.

the inertial mass (30.4 kg). Thus, the structure dynamics for the collocated case between the acceleration (output) and the force (input) can be represented by the sum of N second-order systems as follows [17]

$$G(s) = \sum_{i=1}^{N} \frac{\alpha_i s^2}{s^2 + 2\zeta_i \omega_i s + \omega_i^2}, \tag{1}$$

in which $s = j\omega$, ω is the frequency, N is the number of considered modes in the frequency bandwidth of interest, and $\alpha_i \geqslant 0$, ζ_i and ω_i are the inverses of the modal mass, damping ratio and natural frequency associated to the ith mode, respectively. The experimental FRF was then identified using $N = 1$ in Equation (1) since there is only one vibration mode for the excitation frequency bandwidth (3–4 Hz). A natural frequency of 3.50 Hz was obtained, a damping coefficient of 0.7% and a modal mass of 18 500 kg. These values were finally the parameters used to design the TMD (section 3). Note

DOI: 10.1002/stc

that the value of the natural frequency and damping ratio coincide quite well with those obtained by the OMA (see Table I).

Secondly, the same FRF was obtained using another chirp signal but now with frequency content between 1 and 15 Hz. In that way, the first and third bending modes could be excited. A parameter identification of model (1) was carried out using $N=2$, given

$$G(s) = \frac{5.40 \cdot 10^{-5} s^2}{s^2 + 0.3079s + 483.6} + \frac{5.85 \cdot 10^{-5} s^2}{s^2 + 0.5887s + 3451}. \quad (2)$$

Figure 5 shows the magnitude of the modelled and experimental FRF between 1 and 15 Hz. Higher vibration modes are unlikely to be excited by human excitations. It can be observed that the vibration modes at 6.3 and 7.4 Hz (see Figure 3) are not clearly observed, and they were not considered into the model. It was found that this model captures the structure dynamics with sufficient accuracy for the bandwidth of interest. This model was used for the AVC design (section 4).

2.3. Vibration serviceability assessment

Comfort requirements in codes are handled by provided ranges of structure natural frequencies to be avoided. Thus, structures whose natural frequencies fall outside the provided ranges will generally not be at risk of resonance loading. However, if structure natural frequencies fall into such ranges, further dynamic calculation is required. This consists in evaluating if limit values of acceleration are overcome. Some of the international codes limit the bridge natural frequencies at or just below 3 Hz whereas other codes (such as Appendix 2 of Eurocode 5, BS 5400 or the new Spanish Code for Steel Structures) limits the frequencies at or just below 5 Hz, accounting then for higher harmonics of pedestrian excitation [12]. Therefore, it can be considered that the first bending mode at 3.5 Hz is within the natural frequencies to be a risk of resonance loading (see Figure 3). In particular, the second harmonic of walking and first harmonic of running might excite this vibration mode.

Most of the current design guidelines of footbridges set the comfort limit for the vertical acceleration with a frequency around 3.5 Hz into a range of 0.4 to 1 m/s^2 [23]. These values are associated for a theoretical load of a single synchronised pedestrian. It should be note that these values are conservative if more severe excitations than synchronised walking or running are considered. Following the recommendation given in [12], greater limit values can be permitted for other excitations such as repetitive jumping or groups of joggers. A deterministic model for the vertical force based on its representation in the time domain as a sum of Fourier harmonic components was used.

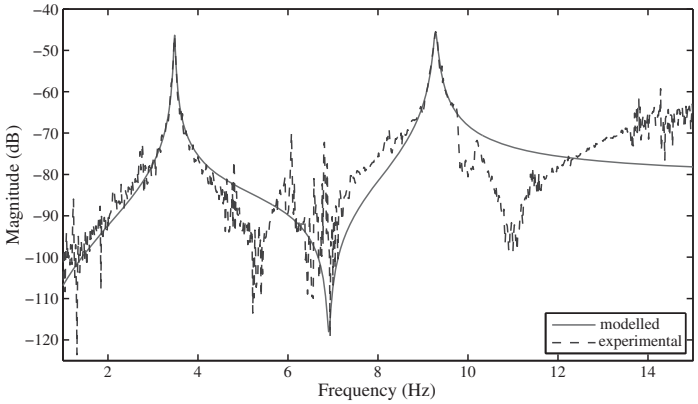

Figure 5. Transfer function of the structure $G(s)$: magnitude in dB referenced to 1 ms^{-2} N^{-1}.

Table II. Structure acceleration for a single synchronised person (of 1000 N) walking and running.

	Simulation	Experimental
Walking at 1.75 Hz	0.39	0.41
Running at 3.5 Hz	6.16	3.34

DOI: 10.1002/stc

A single person of weight 1000 N was considered; the dynamic load factors for the representation of the excitation proposed in [24] were assumed for walking, and those proposed in [25] were assumed for running. Table II shows the structure acceleration values obtained using the aforementioned vertical force models and those obtained experimentally (by a person of 1000 N using a metronome). It was observed that, for a synchronised walker exciting the structure by the second harmonic, the acceleration did not overcome the comfort limit values given by regulations. However, it was found, both theoretically and experimentally, that a synchronised runner may get the structure to overcome the comfort limits clearly. This fact coincided with the general users' opinion since they usually complain about the structural vibrations when runners cross the bridge. Note that the theoretical predicted value is greater than the one obtained experimentally. This might be due to an increase of damping with the response amplitude (nonlinear behaviour of the structure) and due to the possibility of non-perfect synchronisation.

3. PASSIVE CONTROL

This section presents the design and experimental implementation of a TMD at the control point in span 2 designed to reduce the structure response due to the first bending mode (at 3.5 Hz). TMDs are considered an efficient means to add damping to a specific vibration mode into structures prone to vibrations, e.g. bridges and high-rise buildings. Basically, a passive TMD is a secondary mass (also called moving or inertial mass) attached to the structure (main mass) by means of springs and dampers. The TMD mass is fixed as a fraction of the modal mass of the targeted vibration mode (mass ratio); the stiffness of the springs is selected to obtain the optimum TMD frequency, and the viscous dampers ensure the operation of the TMD in a range of frequencies around the tuning frequency. Energy is dissipated by the moving mass inertial force acting on the structure.

3.1. Tuned mass damper design

The optimisation of the TMD parameters was carried out using a methodology based on the design of an H_∞ static output feedback controller [18], which is a method recommended for structures that are excited by mainly periodical loads. This method is just used to optimise the stiffness and damping of the TMD. It should be noted that TMD formulas for structures with vanishing structural damping, such as those obtained by Asami and Nishihara [26], could have been used since the structure damping is small (less than 0.01; see Table I). The feedback system of Figure 6 is assumed to carry out the design. In this figure, $\underline{P}(s)$ is the transfer function matrix of the structure with the TMD attached, $\underline{K}$ is a static matrix of controller gains, w is the disturbance input, $\underline{u}$ is vector of control inputs, z is the controlled output and $\underline{y}$ is the vector of measured outputs. It has been demonstrated [18] that the transfer function matrix of the structure TMD can be transformed into the feedback system of Figure 6 in which the TMD stiffness, k_T, and damping, c_T, play the role of feedback control gains. The optimisation problem obtains k_T and c_T for a given mass ratio (μ) between the TMD mass and the modal mass, such that

$$\min_{k_T, c_T \in \mathbb{R}^+} \left\| \mathrm{G}_{zw}(k_1, c_1, \mu, k_T, c_T) \right\|_\infty, \tag{3}$$

where $\|\cdot\|_\infty$ is the H_∞-norm, G_{zw} is the closed-loop transfer function between z (the acceleration at the control point) and w (pedestrian force) and k_1 and c_1 are the structure stiffness and damping corresponding to the first vibration mode.

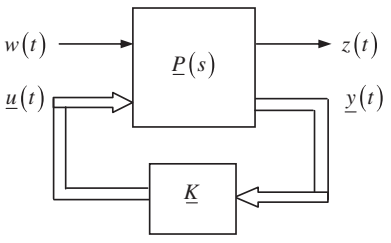

Figure 6. Feedback system.

DOI: 10.1002/stc

Table III. Simulation performance assessment of the TMD previous to its installation. Structure acceleration for a single synchronised person (of 1000 N) walking and running.

Mass ratio	Uncontrolled	0.005	0.01	0.02
Walking at 1.75 Hz				
Acceleration (m/s^2)	0.39	0.073	0.068	0.048
TMD mass displacement (m)	—	±0.002	±0.001	±0.0005
Running at 3.50 Hz				
Acceleration (m/s^2)	6.16	1.15	0.98	0.73
TMD mass displacement (m)	—	±0.029	±0.015	±0.008

The optimization problem given by Equation (3) was run for three values of the mass ratio: $\mu = 0.005$, 0.01 and 0.02. Before the TMD implementation, simulations were performed using these mass ratio values. Table III shows uncontrolled acceleration, the acceleration with TMD and the TMD mass displacement for walking at 1.75 Hz and running at 3.5 Hz. The moving mass displacement was important since the space under the walkway was limited. This available displacement was predicted from an initial conceptual design to be ±0.05 m (see Figure 7). Eventually, it was decided to use a mass ratio of 1%, $\mu = 0.01$, which was enough to keep the structure with acceptable level of vibrations, and the maximum displacement available was not overtaken with sufficient safety margin. The parameters obtained for the TMD were as follows: $k_T = 87\,015$ N/m and $c_T = 537$ Ns/m, which is equivalent to a frequency of 21.67 rad/s (3.45 Hz) and a damping ratio of 0.067.

3.2. Implementation of the tuned mass damper

The physical design of the TMD was carried out, taking into account the design parameters and the space limitation under the walkway, where the TMD was planned to be installed. Figure 7a shows the cross section of the bridge and the available space under the deck. A computer-aided design (CAD) model of the TMD is depicted in Figure 7b (more details about its physical implementation can be found in [27]). The TMD consists of a steel tray to place steel plates (10, 5, 2, 1 kg), four helical steel springs to suspend the mass and two viscous dampers. Also, various rubber stroke limits were placed in order to avoid excessive mass movements and keep the TMD safe. Four helical springs with a stiffness of 21 900 N/m each were used (SPEC-BARNES DH14330), (Barnes Group Inc., Bristol, USA) giving a final stiffness of 87 600 N/m (close to the optimal value). Two viscous dampers were designed, consisting merely in a piston submerged into a pot with viscous fluid. An experimental identification of the damping coefficient was carried out, resulting in approximately 260 Ns/m. Hence, both dampers together provided approximately the optimal TMD damping. The installation of the TMD under the timber deck and a detail view of the TMD are shown, respectively, in Figure 8a and b. Since the performance of TMDs is relatively insensitive to the damping, it was decided to modify *in situ* the TMD frequency, which is crucial for the system performance, by changing the TMD mass (just by changing the steel plates sited on the tray of the TMD).

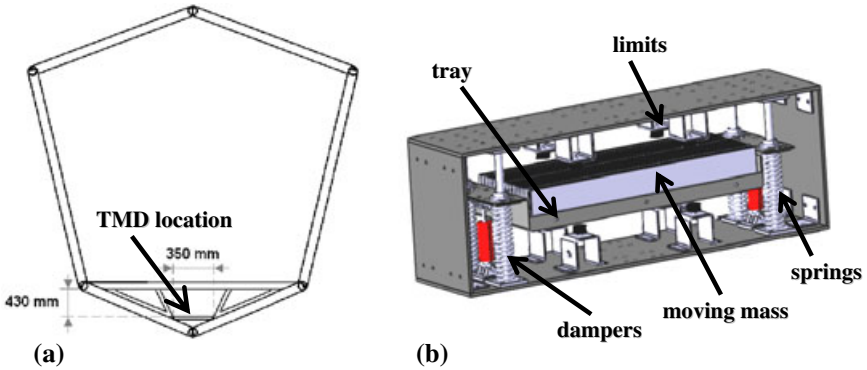

Figure 7. (a) Footbridge cross section and TMD location under the timber walkway. (b) CAD model of the TMD.

DOI: 10.1002/stc

An *in situ* tuning of the TMD frequency value was carried out by obtaining several experimental FRFs (changing the TMD mass) between the structure acceleration and the input force with the TMD installed. These FRFs were undertaken as were carried out for the structure identification (subsection 2.2). That is, the same electrodynamics shaker was employed to provide a controlled input. Finally, the TMD mass used was 187 kg. Figure 9 shows the magnitude of the FRF for the final TMD mass selected. Additionally, the theoretical FRF and the uncontrolled one are included for comparison. As can be observed, the TMD was well tuned. Eventually, several extreme excitations such as perfectly synchronised running and jumping at the targeted frequency were carried out to check that the moving mass did not hit the limits.

4. ACTIVE CONTROL

This section describes the identification of the actuator dynamics and the design and experimental implementation of an AVC system via a proof-mass actuator on the test structure. The methodology used here, CAFC, has been recently presented in [16] for human-induced vibration cancellation in an office floor and has been used in this work for a footbridge. An AVC of a lively footbridge has been recently carried out in [13]. However, the obtained results were of limited relevance since the control law employed (DVFC) did not consider the interaction between structure and actuator dynamics. The methodology used here accounts for the interaction between structure and actuator dynamics and also accounts for stroke saturation and force overloading.

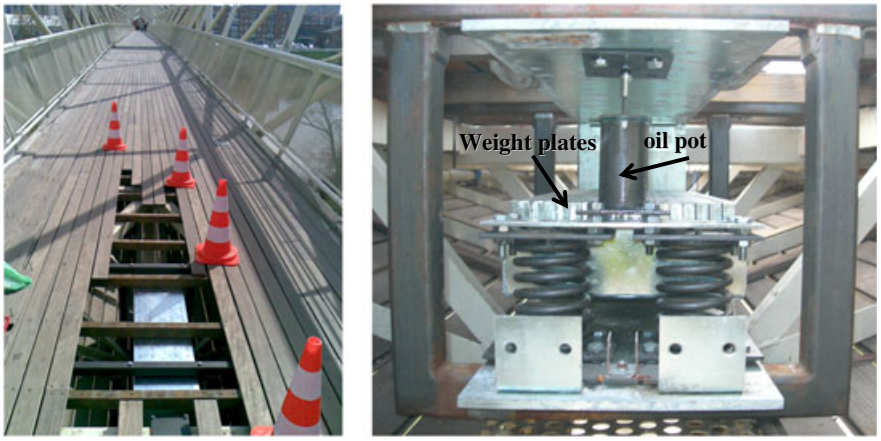

Figure 8. (a) TMD installation. (b) Detailed view.

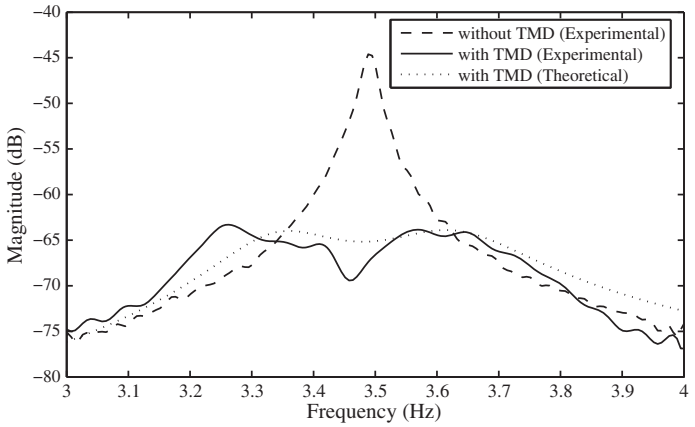

Figure 9. Experimental transfer function of the structure without and with TMD.

DOI: 10.1002/stc

4.1. Proof-mass actuator dynamics

The same shaker (APS Dynamics Model 400) that was used to obtain the FRFs for the structure (subsection 2.2) was used as inertial actuator for the AVC implementation. An inertial actuator (also known as proof-mass actuator) generates inertial forces in the structure on which it is placed without the need for a fixed reference. The actuator consists of a reaction (moving) mass attached to a current-carrying coil moving in a magnetic field created by an array of permanent magnets. The moving mass is connected to the frame by a suspension system. Thus, the transfer function between the inertial force applied to the structure and the input voltage can be closely described as a linear third-order model [17]. This transfer function was identified using voltage-driven mode as

$$G_{\mathrm{A}}(s) = \left(\frac{K_{\mathrm{A}} s^2}{s^2 + 2\zeta_{\mathrm{A}}\omega_{\mathrm{A}} s + \omega_{\mathrm{A}}^2}\right)\left(\frac{1}{s+\varepsilon}\right) = \frac{22\,400 s^2}{s^3 + 135.4 s^2 + 519.4 s + 8803}, \tag{4}$$

in which $\omega_{\mathrm{A}} = 8.17$/rad (1.3 Hz) is the natural frequency associated with the suspended moving mass and $\zeta_{\mathrm{A}} = 0.21$ is the damping ratio. The pole at $-\varepsilon$ accounts for the low-pass property exhibited by these actuators. A cut-off frequency of 21 Hz ($\varepsilon = 2\pi \cdot 21 = 131.94$) was identified for this low-pass element. Figure 10 shows the magnitude of the modelled and experimental FRF between 0 and 30 Hz.

4.2. Active vibration control design

The main components of the control strategy adopted in this work are shown in Figure 11. The output of the system is the structural acceleration since this is usually the most convenient quantity to measure. Because it is rarely possible to measure the system state and due to simplicity reasons, direct output measurement feedback control might be preferable rather than state-space feedback in practical problems [28]. In the control scheme, G_{A} is the transfer function of the actuator (Equation (4)), G is of the structure (Equation (2)), C_{F} is of a feedback compensator and C_{D} is of a direct compensator. The feedback one is a phase-lag compensator (first-order compensator) designed to increase the closed-loop system stability and to make the system more amenable to the introduction of significant damping by a closed-loop control. The direct one is merely a phase-lead compensator (high-pass property) designed to avoid actuator stroke saturation for low-frequency components. It is notable that its influence on the global stability will be small since only a local phase-lead is introduced. The control law is completed by a nonlinear element $f(\dot{y}_{\mathrm{c}})$ that may be a saturation nonlinearity to account for actuator force overloading [16] or an on–off nonlinearity with a dead zone [15]. In this work, a saturation nonlinearity was assumed.

The design process presented in [16] was followed. The steps for the design process are as follows: (i) identify the actuator G_{A} and structure dynamics G; (ii) design C_{D} to reduce the sensitivity of the actuator to stroke saturation; (iii) design C_{F} to increase the damping and robustness with respect to stability and performance of the closed-loop system; and (iv) select a control gain using the root locus

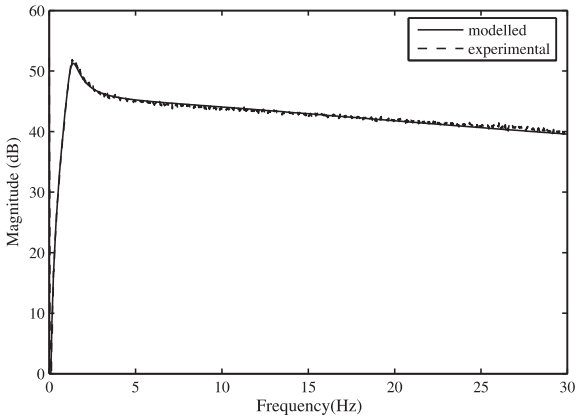

Figure 10. Transfer function of the actuator $G_{\mathrm{A}}(s)$: magnitude in dB referenced to 1 N/V.

DOI: 10.1002/stc

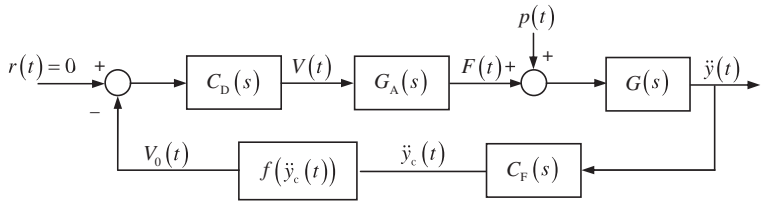

$r(t)$	Reference command	$\ddot{y}(t)$:	Acceleration response
$V(t)$:	Control voltage	$\ddot{y}_c(t)$:	Compensated acceleration
$F(t)$:	Actuator force	$V_0(t)$:	Initial control voltage
$p(t)$:	Plant disturbance	$f(\ddot{y}_c)$:	Nonlinear element
$C_D(s)$:	Transfer function of the direct compensator		
$G_A(s)$:	Transfer function of the proof-mass actuator		
$G(s)$:	Transfer function of the structure		
$C_F(s)$:	Transfer function of the feedback compensator		

Figure 11. General control scheme.

method and design the nonlinear element $f(\ddot{y}_c)$ to avoid force overloading. A direct compensator of the form

$$C_D(s) = \frac{s+\lambda}{s+\eta} \quad \text{with} \quad \eta > \lambda \geq 0, \tag{5}$$

is applied to the initial control voltage $V_0(t)$, and its output is the filtered input to the actuator $V(t)$ (see Figure 11). A maximum stroke for harmonic excitation of 0.05 m was considered in the design, which is appropriate considering that the actual stroke limit of the actuator is 0.075 m. The controller parameters were found to be $\lambda = 5.6$ and $\eta = 24.6$. These parameters are selected in such a way that the likelihood of stroke saturation is reduced significantly. The stroke saturation leads to collisions of the inertial mass with its stroke limits, imparting highly undesirable shocks to the structure and possibly causing damage to the actuator.

Once the direct compensator is designed, the feedback one is designed considering the dynamics of the actuator, the structure and the direct compensator dynamics. The feedback compensator is of the following form

$$C_F(s) = \frac{s+\gamma}{s} \quad \text{with} \quad \gamma \geqslant 0. \tag{6}$$

Note that if $\gamma = 0$, the control scheme will be direct acceleration feedback, and if $\gamma >> \varepsilon$ (see Equation (4)), which means that the zero of the compensator does not affect the dominant system dynamics, the control scheme will then be considered DVFC. Parameter γ has to be chosen according to the closed-loop poles corresponding to the first natural frequency of the structure in order to (i) improve substantially their relative stability; (ii) decrease their angles with respect to the negative real axis to allow increasing damping; and (iii) increase the distance to the origin to allow increasing natural frequency. Note that increasing values both of the frequency and the damping result in decreasing the settling time of the corresponding dynamics [29]. $\gamma \geqslant 35.5$ was obtained. A value of $\gamma = 50$ was finally chosen.

The root locus technique was then used. The root locus maps the complex linear system roots of the closed-loop transfer function for control gains (K_c) from zero (open-loop) to infinity. The root locus of the total transfer function of the linear part $G_T(s) = C_D(s)G_A(s)G(s)C_F(s)$ is plotted in Figure 12a. It can be observed that a couple of branches in the root locus corresponding to the actuator dynamics go to the right-half plane provoking unstable behaviour in the actuator (see Figure 12b). The gain for which the control system is unstable is the limit gain. A limit gain of $K_{c,\,limit} = 82$ V/(m/s^2) was obtained. Finally, a gain of $K_c = 40$ V/(m/s^2) was finally chosen. This gain increases substantially the damping of

DOI: 10.1002/stc

the structure and keeps the poles corresponding to the actuator far away from the imaginary axis. The saturation nonlinearity is as follows

$$f(\dot{y}_c(t)) = \begin{cases} K_c \dot{y}_c(t) & |\dot{y}_c(t)| \le V_s/K_c \\ V_s \text{sign}(\dot{y}_c(t)) & |\dot{y}_c(t)| > V_s/K_c \end{cases}, \tag{7}$$

where K_c is the aforementioned control gain and V_s is the maximum allowable control voltage to the actuator (saturation level). The saturation level was set to $V_s = 1$.

Once both compensators and the control were selected, simulations were carried out in order to assess the AMD performance. MATLAB/SIMULINK (MathWorks, Inc.) was used for this purpose. The same walking and running reaction force models employed for Tables II and III are used here. Table IV shows controlled acceleration response for walking and running excitation. Moreover, the AMD displacement estimation is included.

4.3. Active vibration control implementation

The shaker used for modal identification (section 2), operated in inertial mode, was used as the proof-mass actuator. The response of the structure (the system output) was measured using one of the piezoelectric accelerometers used for the modal identification. The dynamics introduced by the sensor were not considered in the control scheme since they are negligible for the bandwidth of interest. A digital computer was used for the on-line calculation of the control signal $V(t)$. The system output was

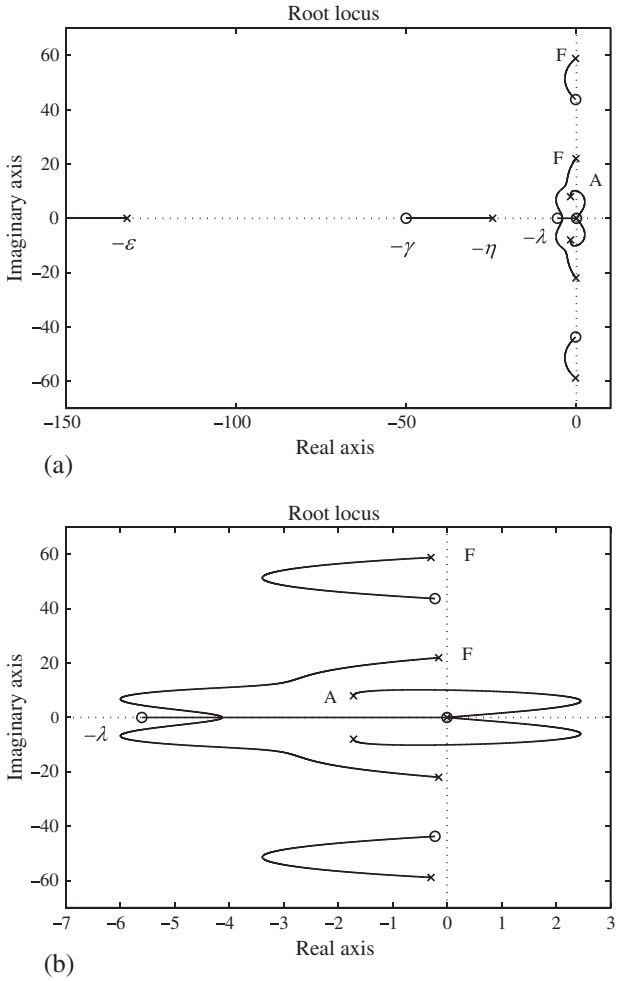

Figure 12. (a) Root locus of the total transfer function $G_T = C_D G_A G C_F$. (b) Zoom of the origin. (×) pole; (o) zero; (F) Footbridge; (A) Actuator.

DOI: 10.1002/stc

Table IV. Simulation performance assessment of the AMD previous to its installation. Structure acceleration for a single synchronised person (of 1000 N) walking and running.

	Uncontrolled acceleration	Acceleration with AMD	AMD mass displacement
Walking at 1.75 Hz	0.39	0.04	±0.034
Running at 3.50 Hz	6.16	3.75	±0.022

sampled with a period of 0.001 s, and the control signal was calculated once every sampling period. Then, the discrete-time control signal was converted into a zero-order-hold continuous-time signal. Likewise, the continuous transfer functions of the compensators were converted to discrete transfer functions using the zero-order-hold approximation. The controller hardware comprises a low-cost embedded digital controller (NI PXI-8101 (National Instruments PXI-8101 CELERON 575 2.0 GHz REAL-TIME)) with a data acquisition card installed (NI PXI-6221 (National Instruments PXI-6221 M Series DAQ)).

5. EXPERIMENTAL RESULT

Walking, running and jumping tests were carried out to assess the efficacy of the control devices designed. The walking tests consisted of walking at 1.75 Hz such that the first vibration mode of the structure (3.5 Hz) could be excited by the second harmonic of walking. A frequency of 3.5 Hz was used for the running tests so that the structure was excited by the first harmonic of running. Jumping tests at 1.75 and 3.50 Hz were also considered. Even though jumping might be considered as a vandalism excitation, it was also used to assess the performance of the control systems. The walking/running tests consisted of walking/running from one end of span 2 to the other and back again. The jumping tests consisted of jumping close to the control point during 30 s and suddenly stopping, allowing thus free decay response of the structure. The pacing frequency was controlled using a metronome set to 105 beats per minute (bpm) for 1.75 Hz and to 210 bpm for 3.5 Hz. Each test was repeated three times. All the tests were carried out by a person of approximately 1000 N.

The results are compared by means of the maximum peak acceleration and the maximum transient vibration value (MTVV) computed from the 1-s running root mean square (RMS) acceleration [30]. Table V shows the result obtained for the four excitations and considering the uncontrolled and controlled cases (TMD and AMD). It is observed that the AMD designed (with a moving mass of 30 kg) performs well (from 67% to 80% reduction in terms of the MTVV) for walking, running and jumping at 1.75 Hz; however, the performance for jumping at the resonant frequency is poor (24% reduction). This is due to the fact that the maximum actuation force is limited by the maximum force provided by the actuator (400 N at 3.5 Hz), which is much smaller than the first harmonic of the vertical reaction force caused by a jumper of 1000 N [31]. The TMD designed (with a moving mass of 187 kg) was shown to be effective for all the excitations (from 65% to 84% reduction in terms of the MTVV) except for walking (33% reduction). This is due to the fact that the TMD performance is poor if the vibration amplitude is

Table V. Experimental performance assessment for walking, running and jumping excitation.

	Uncontrolled	TMD	Reduction (%)	AMD	Reduction (%)
Walking at 1.75 Hz					
Peak acceleration (m/s^2)	0.41	0.25	39	0.16	70
MTVV [a] (m/s^2)	0.21	0.14	33	0.06	67
Running at 3.50 Hz					
Peak acceleration (m/s^2)	3.34	0.85	74	1.19	64
MTVV (m/s^2)	2.20	0.35	84	0.69	68
Jumping at 1.75 Hz					
Peak acceleration (m/s^2)	2.28	0.45	80	0.59	74
MTVV (m/s^2)	1.35	0.24	82	0.26	80
Jumping at 3.50 Hz					
Peak acceleration (m/s^2)	3.41	1.40	59	3.06	10
MTVV (m/s^2)	2.31	0.81	65	1.75	24

[a]Maximum transient vibration value defined as the maximum value of the 1-s running RMS acceleration.

DOI: 10.1002/stc

low, causing thus very low control force from the moving mass. Figure 13 shows the response time histories (including the 1 s RMS) uncontrolled and controlled by the TMD and the AMD for a walking test. Figure 14 shows the same plots for a running test. A set of recorded response time histories for a jumping test at 3.5 Hz is depicted in Figure 15. Finally, Table VI shows the damping ratios estimated from the free motion of the structure obtained after each jumping test. The logarithmic decrement method was used for the estimation. Interestingly, the damping ratios obtained for jumping test with the AMD were greater than those obtained with the TMD, even for the case of jumping at 3.5 Hz. That is, when the AVC system is used, the vibration drops off more quickly (see Figure 15b and c).

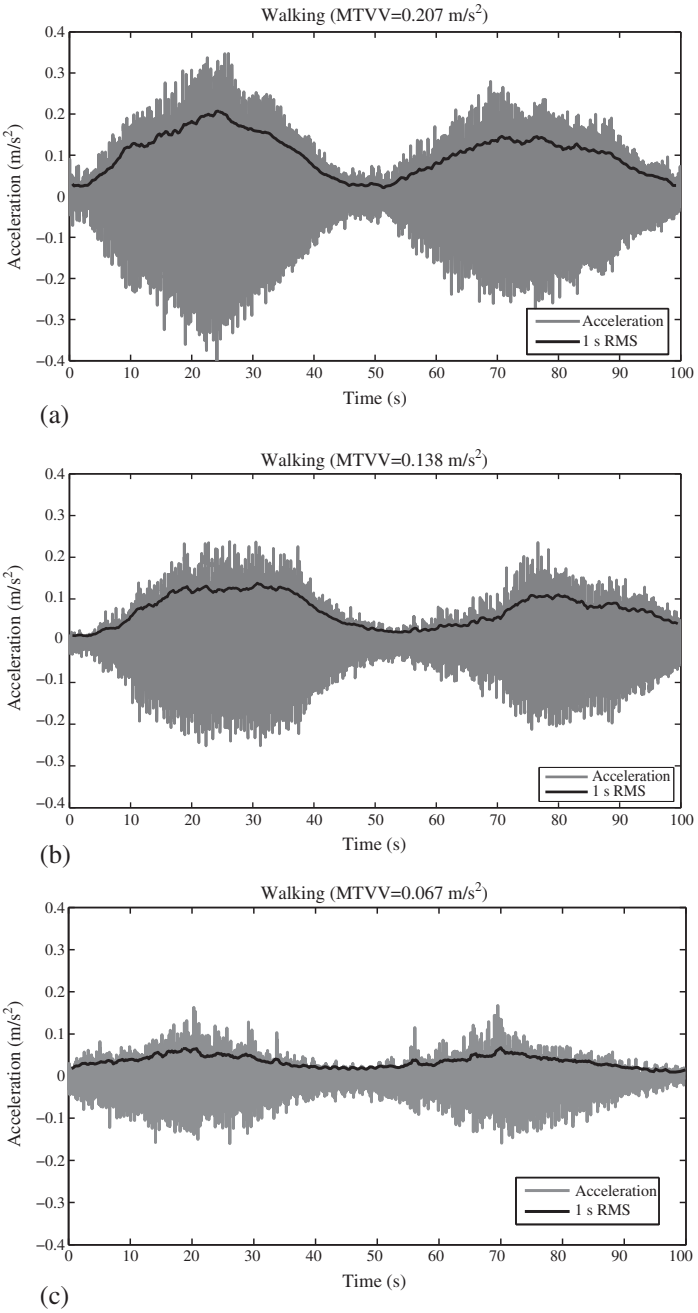

Figure 13. Walking test. (a) Uncontrolled. (b) Controlled by the TMD. (c) Controlled by the AMD.

DOI: 10.1002/stc

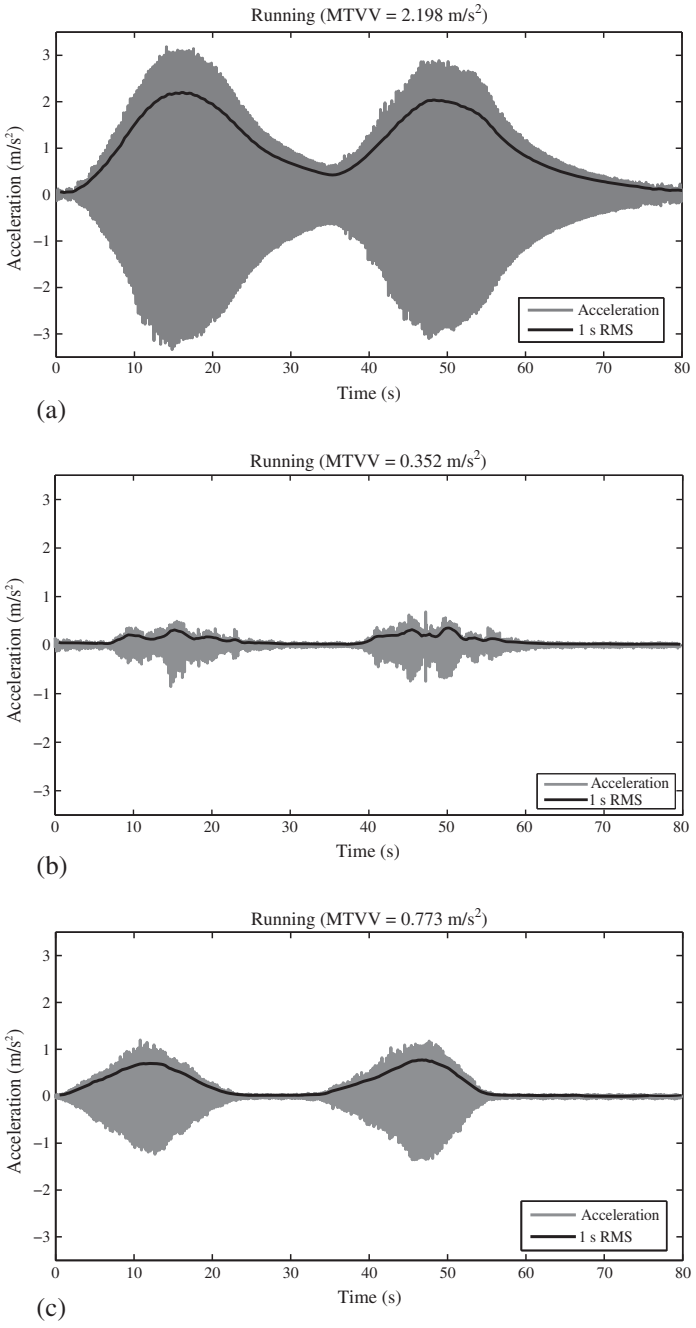

Figure 14. Running test. (a) Uncontrolled. (b) Controlled by the TMD. (c) Controlled by the AMD.

6. DISCUSSION AND CONCLUSIONS

The control of human-induced vibrations on an in-service footbridge has been addressed throughout this paper. The test structure is an urban footbridge representative of lightweight structure susceptible to human-induced vibrations. Once the dynamic properties of the structure were identified, the design and implementation of two different control techniques based on passive and active control were carried out. The passive control has been performed using a TMD, which is the most common solution adopted to improve the dynamic behaviour of footbridges. The TMD was designed using an H_∞ approach that takes into account the damping of the structure. The active control has been addressed through the use of a commercial electrodynamic shaker controlled by an acceleration feedback-based strategy.

DOI: 10.1002/stc

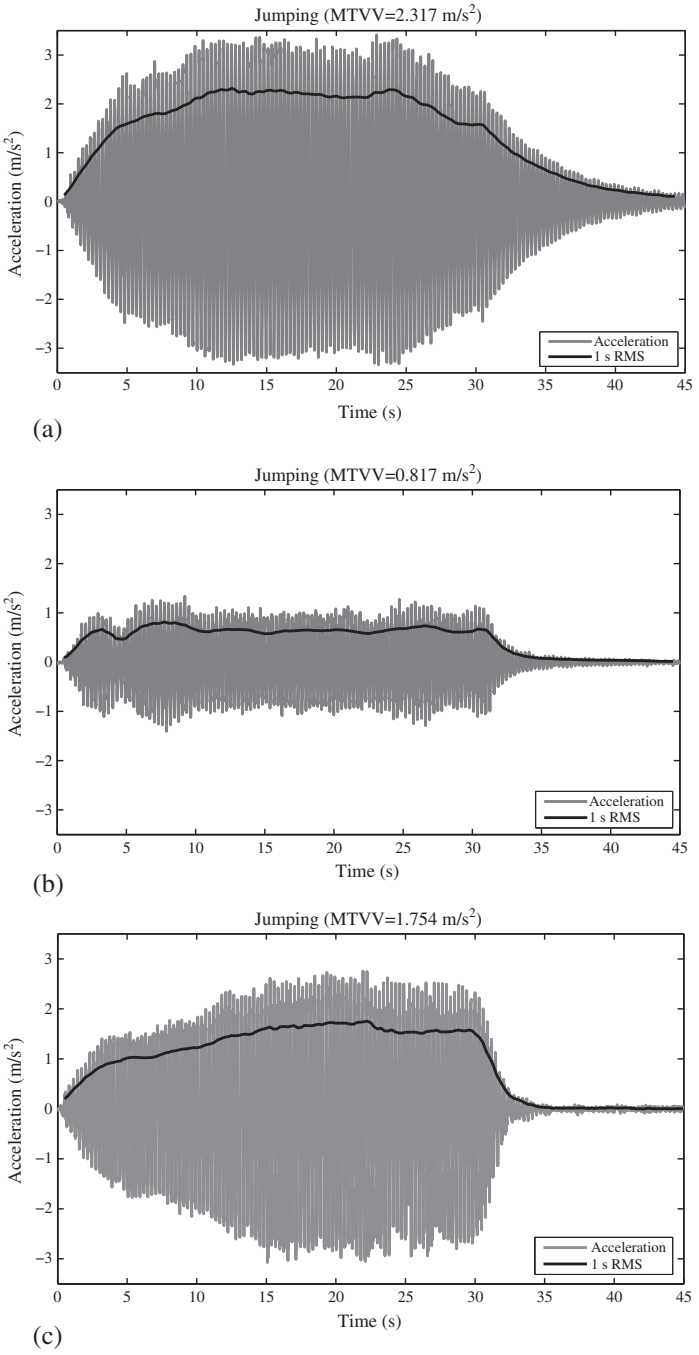

Figure 15. Jumping test at 3.5 Hz. (a) Uncontrolled. (b) Controlled by the TMD. (c) Controlled by the AMD.

The vibration control via a TMD, which is a well-established technology, has been addressed successfully. Since the structure has one dominant vibration mode (which is well separated from the others) prone to be excited by human loading, the TMD has been an economical and effective solution as expected. Vibration reductions between 40% and 80% have been achieved for all the excitation considered using a TMD mass of 185 kg, 1% of the modal mass (Table V). Apart from the initial budget, the maintenance costs are, in principle, low. However, the TMD mass has to be fine-tuned periodically since structural natural frequencies change with structural ageing. Further, environmental conditions (mainly temperature and wind) [32] and pedestrian density [33] might change the resonance response of the structure, thus affecting the TMD performance.

DOI: 10.1002/stc

Table VI. Damping ratio, as a percentage of critical damping, obtained from the free decay after suddenly stopping the jumping test.

	Uncontrolled (%)	TMD (%)	AMD (%)
Jumping at 1.75 Hz	0.72	2.37	3.30
Jumping at 3.50 Hz	0.91	2.39	3.53

As for the authors' knowledge, this has been the first successful implementation of AVC on an in-service footbridge. The actuator was a commercial shaker with a 30-kg inertial mass controlled by a low-cost acquisition card. Vibration reductions between 60% and 80% have been achieved for all the excitation considered except for jumping at the structure natural frequency for which the reduction was 20% (Table V). It has been observed that both systems were of similar efficacy for a synchronised runner and that the AVC shows better performance for low-amplitude vibration (a synchronised walker). That is, the AVC has been shown to be more robust with respect to performance. It should be noted that the inertial mass value of the AVC was more than six times smaller than the TMD one.

It has been shown that active control could be a realistic and reasonable solution for flexible lightweight civil engineering structures such as lively footbridges or lightweight floor structure [16]. In these cases, in which low control forces are required (as compared with other civil engineering applications such as high-rise buildings or long-span bridges), electrical actuators can be employed. These actuators present advantages with respect to hydraulic ones such as lower cost, maintenance and level of noise. However, AVC systems for human-induced vibrations needs much further research and development to jump into building and construction technologies considered by designers. With respect to passive systems, such as the TMD developed in this work, cost is still the major disadvantage. Considering the two vibration control systems developed in this work, the AVC hardware and installation might be estimated to cost between three and four times more than the passive one. Additionally, the energy consumption was estimated to be between 1000 and 2000 kWh per year, which is approximately the energy consumption of one or two electric bulbs of 100 W continuously plugged in. Then, the energy consumption is not a drawback for electrodynamics actuators. Additionally, there is no need of re-tuning the system periodically. It is expected that this technology will become less expensive and more reasonable in the near future. Research projects involving the development of new affordable and compact actuators for human-induced vibration control are currently on the go [34].

The authors are currently working on a permanent implementation of the AVC strategy presented in this work. It is planned to evaluate the AVC performance and energy consumption through long-term monitoring results. Moreover, the research carried out herein has made the investigation on AVC strategies more efficient and economically interesting. Future developments will consider control laws in which the inertial mass displacement will be included to improve the system efficacy, and a switching-off function will also be included in order to disconnect the system when the acceleration level is under the allowable threshold (given by design guidelines).

ACKNOWLEDGEMENTS

The authors would like to acknowledge the support of the Science Museum personnel and Valladolid City Council. Dr. Iván M. Díaz would like to acknowledge the financial support of Universidad de Castilla-La Mancha (Short-Stay Visitor Grant Program) and the Consejería de Ciencia y Tecnología of Junta de Comunidades de Castilla-La Macha (Research Grant PPII11-0189-9976).

REFERENCES

1. Bachmann H. Case studies of structures with man-induced vibrations. *Journal of Structural Engineering* 1992; **118**:631–647.
2. Bachmann H. Lively footbridges—a real challenge. *Proceedings of the International Conference on the Design and Dynamic Behaviour of Footbridges*. OTUA: Paris, France, 2002.
3. Hanagan LM, Raebel CH, Trethway MW. Dynamic measurements of in-place steel floors to assess vibration performance. *Journal of Performance of Constructed Facilities* 2003; **17**:126–135.
4. Willford M. Dynamic actions and reactions of pedestrians. *Proceedings of the International Conference on the Design and Dynamic Behaviour of Footbridges*. OTUA: Paris, France, 2002.

DOI: 10.1002/stc

5. Mimram M. Towards reasoned, open-minded footbridge design. *Proceedings of the International Conference on the Design and Dynamic Behaviour of Footbridges*. OTUA: Paris, France, 2002.
6. Soong TT, Spencer BF, Jr. Supplementary energy dissipation: state-of-the-art and state-of-the-practice. *Engineering Structures* 2002; **24**:243–159.
7. Caetano E, Cunha A, Moutinho C, Magalhães, F. Studies for controlling human-induced vibration of the Pedro e Inês footbridge, Portugal. Part 2: Implementation of tuned mass dampers. *Engineering Structures* 2010; **32**:1082–1091.
8. Occhiuzzi A, Spizzuoco M, Ricciardelli F. Loading models and response control of footbridges excited by running pedestrians. *Structural Control and Health Monitoring* 2008; **15**:349–368.
9. Lee CL, Chen YT, Chung LL, Wang YP. Optimal design theories and applications of tuned mass dampers. *Engineering Structures* 2006; **28**:43–53.
10. Zuo L. Effective and robust vibration control using series multiple tuned-mass dampers. *ASME Journal of Vibration and Acoustics* 2009; **131**:031003.
11. Reiterer M, Ziegler F. Control of pedestrian-induced vibrations of long-span bridges. *Structural Control and Health Monitoring* 2006; **13**:1003–1027.
12. FIB-Bulletin 32. Guidelines for the design of footbridges. *International Federation for Structural Concrete*, Lausanne, Switzerland, 2005.
13. Moutinho C, Cunha A, Caetano E. Analysis and control of vibrations in a stress-ribbon footbridge. *Structural Control and Health Monitoring* 2011; DOI: 10.1002/stc.390
14. Balas MJ. Direct velocity feedback control of large space structures. *Journal of Guidance and Control* 1979; **2**:252–253.
15. Díaz IM, Reynolds P. On–off nonlinear active control of floor vibrations. *Mechanical Systems and Signal Processing* 2010; **24**:1711–1726.
16. Díaz IM, Reynolds P. Acceleration feedback control of human-induced floor vibrations. *Engineering Structures* 2010; **32**:163–173.
17. Preumont A. *Vibration Control of Active Structures: An introduction*. Kluwer Academic: Dordrecht, The Netherlands, 1997.
18. Poncela A, Casado CM, Baeyens E, Perán JR. Design of devices to protecting civil infrastructures using fixed-order H_∞ control. *Structural Control and Health Monitoring* 2007; **14**:239–260.
19. Díaz IM, Casado CM, de Sebastián J. Active vibration control study of an in-service footbridge using an inertial proof-mass actuator. *Proceedings of Fifth World Conference on Structural Control and Monitoring*, paper 272, Tokyo, Japan, 2010.
20. Gómez M. A new and unusual cable-stayed footbridge at Valladolid (Spain). *Steelbridge 2004: Symposium International sur les Ponts Metálliques*, Milau, France, 23–25 June, 2004.
21. Martínez J, Gómez M. The versability of stay bridges. *Solids and Structures* 2004; **220**:4–5.
22. ARTeMIS. Structural Vibration Solutions. Available at www.svibs.com, 2010.
23. Sétra. Technical guide footbridges. Assessment of vibrational behaviour of footbridges under pedestrian loading. Service d'études techniques des routes et autorutes, Paris, France, 2006.
24. Young P. Improved floor vibration prediction methodologies. *Arup Vibration Seminar on Engineering Structural Vibration—Current Developments in Research and Practice*, Institution of Mechanical Engineers, London, U.K., 4 October 2001.
25. Bachmann H, Pretlove AJ, Rainer H. Dynamic forces from rhythmical human body motions. *Vibration Problems in Structures: Practical Guidelines*, Appendix G, Birkhäuser: Basel, Switzerland, 1995.
26. Asami T, Nishihara O. Closed-form exact solutions to H-infinity optimization of dynamic vibration absorbers (application to different transfer functions and damping systems). *ASME Journal of Vibration and Acoustics* 2003; **125**:398–405.
27. Casado CM, de Sebastián J, Díaz IM, Poncela A. Vibration serviceability assessment and passive vibration control of a lively footbridge. *Proceedings of Fifth World Conference on Structural Control and Monitoring*, paper 249, Tokyo, Japan, 2010.
28. Chung LY, Jin TG. Acceleration feedback control of seismic structures. *Engineering Structures* 1998; **20**:62–74.
29. Bolton W. *Control Engineering*. Logman: United Kingdom, 1998.
30. ISO 2631–1. *Mechanical Vibration and Shock—Evaluation of Human Exposure to Whole-body Vibration, Part 1, General Requirement*. International Organization for Standardization: Switzerland, 2008.
31. Racic V, Brownjohn JMW, Pavic A. Reproduction and application of human bouncing and jumping forces from visual marker data. *Journal of Sound and Vibration* 2010; **239**:3397–73416.
32. Sohn H. Effects of environmental and operational variability on structural health monitoring, *Philosophical Transactions of The Royal Society A* 2007; **365**:539–560.
33. Živanović S, Díaz IM, Pavić A. Influence of walking and standing crowds on structural dynamic properties. *Proceedings of the XXVII International Modal Analysis Conference*, paper 53, February 9–12, Orlando, Florida USA, 2009.
34. Research Grant EP/H009825/1. Active control of human-induced vibration, PI: Dr Paul Reynolds, Engineering and Physical Sciences Research Council, United Kingdom, 2010–2012.